Effects of high-temperature thermal annealing on GeSn thin-film material and photodetector operating at 2 µm

Shaoteng Wu,[1*] Bongkwon Son,[1] Lin Zhang,[1] Qimiao Chen,[1] Hao Zhou,[1] Simon Chun Kiat Goh[1] and Chuan Seng Tan.[1,2*]

[1]School of Electrical and Electronic Engineering, Nanyang Technological University, 50 Nanyang Avenue, Singapore 639798

[2]Low Energy Electronic Systems (LEES), Singapore-MIT Alliance for Research and Technology (SMART), Singapore 138602

*E-mail: shaoteng.wu@ntu.edu.sg; TanCS@ntu.edu.sg

Highlights

1. Ordered nanopatterns are formed on the surface of GeSn from high-temperature annealing (~700°C).
2. Structural and optical properties of GeSn films before and after rapid thermal annealing are reported.
3. The decrease of the dark current with an enhancement of the I_p/I_d ratio (on-off ratio) indicates an improvement of the photodetector detectivity due to the annealing process at ~700°C
4. An increased photocurrent (>200%) is observed for the GeSn photodetector at an annealing temperature of 550°C at 2-μm wavelength.

Abstract

Here, we explore the thermal stability of GeSn epilayers with varying Sn contents (3-10%) at an annealing temperature ranging from 300 to 750°C. It is found that ordered nanopatterns are formed on the surface of GeSn with Sn content of 8% without excessive Sn precipitation after thermal annealing at 700°C. Despite being annealed at high temperatures, the GeSn maintains its crystal structure, which is confirmed by the X-ray Diffraction (XRD), Raman spectrum, and secondary-ion mass spectrometry (SIMS). The corresponding photocurrents of the photodetectors at the wavelength of 2 μm also indicate the crystal quality of the GeSn alloys does not deteriorate significantly after high-temperature annealing (675-700°C). Meanwhile, the decrease of dark current with the enhancement of I_p/I_d ratio (on-off ratio) indicates the improvement of detectivity of the photodetector due to the annealing process. Furthermore, the annealing temperature is optimized to 550°C to achieve 200% enhancement of photocurrents of the GeSn photodetectors operated at 2 μm.

Keywords: GeSn alloy, annealing, structural property, nanopattern, infrared photodetector

1. Introduction

Germanium-tin (GeSn) is a promising material for extending the applications of the current silicon-based electronic device technologies due to its excellent carrier mobility and bandgap tunability [1-3]. However, the low thermoequilibrum solubility of Sn in Ge (less than 1% at Ge-Sn eutectic of 231°C) makes the introduction of high Sn contents in a Ge matrix difficult due to Sn segregation or precipitation. Recently, single-crystal GeSn layers with high Sn contents have been realized by non-equilibrium growth techniques such as chemical vapor deposition (CVD) [4-6], molecular beam epitaxy (MBE) [7, 8], and sputtering epitaxy [9]. However, the low growth temperature of these methods for avoiding Sn segregation is the major obstacle to obtain device-grade GeSn materials due to the introduction of point defects [10], which are detrimental to its electronic and optoelectronic applications.

Thermal annealing, the widely used technique for relaxing strain and improving crystal quality, has been untilized to improve the GeSn film quality [11-13]. The thermal annealing process does not only decrease the defect density and improve the optical quality [14] but could also increase the portion of substitutional Sn atoms in the GeSn layer [15]. Contrary to that of SiGe system, the crystallinity of high-Sn content GeSn always deteriorates during the thermal annealing process. Numerous efforts have been attempted to clarify the relationship between the Sn segregation and strain relaxation and/or misfit dislocation [12, 16-19]. Many reports have suggested that the critical annealing temperature should be less than 600°C to avoid the Sn segregation after the strain relaxation [12, 14, 20].

The 2 μm communication band has been suggested as a promising solution for the projected ‘capacity crunch’ of conventional single-mode fibers (SMFs). GeSn alloy offers an alternative approach from III-V materials to extend the detection range of Ge towards 2 μm. Recently, GeSn photodiodes operated at 2 μm have been demonstrated on different platforms (Si, Ge, and Si-on-insulator) [3, 21, 22]. However, the performance of the GeSn photodiodes at 2 μm is relatively low compared to the III-V photodiode, mainly due to the high-density defect generated from the low-temperature growth process. Thus, similar to other materials the post thermal annealing could be a solution to decrease the defect density of GeSn and improve its photodetector performance at 2 μm. Yet, to our best knowledge, there is no previous work that reports the effects of thermal annealing on the performance of a single-crystal GeSn photodetector.

In this paper, GeSn layers with varying Sn contents that range from 3 to 10% are investigated. Rapid thermal annealing (RTA) with temperatures ranging from 300 to 750°C is carried out. Contrary to the previous research, we observed that highly ordered nanopatterns are formed on the surface of GeSn with Sn content of 8% after strain relaxation at an annealing temperature of 700°C. No usual excessive Sn precipitation was observed. Despite the use of high annealing temperature, the GeSn structure did not severely damage, as confirmed by the XRD, micro-Raman spectroscopy. Thereafter, the effect of the annealing process on the performance of the photodetector made from the GeSn film will also be presented. We demonstrated that an optimized annealing temperature significantly enhances the photocurrent of the GeSn photodetector (>200%) at the wavelength of 2 μm.

2. Experimental

GeSn films with Sn contents ranging from 3.3 to 10.0% were grown on strain relaxed Ge buffer layer with a thickness of 850 nm on 6” Si (100) substrates in a reduced pressure chemical vapor deposition (RPCVD) chamber (ASM E2000 reactor). The growth temperature ranges from 290 to 325°C and the growth duration was fixed at 10 mins. The thicknesses of the GeSn films grown with Sn content of 3.3, 8, and 10% are 180, 195, and 170 nm, respectively, as confirmed by XRD and secondary ion mass spectrometry (SIMS). Subsequently, the GeSn wafers were cut into smaller pieces (1.5 cm×1.5 cm) and annealed in an RTA system (AnnealSys AS-One) at various temperatures ranging from 350 to 750°C in the nitrogen ambient. For the RTA process, a thermocouple was used to monitor the temperature in real-time. The annealing time is 1 min unless otherwise mentioned.

The structural and strain evolution of annealed GeSn films were analyzed by XRD using CuKα1 (λ_{XRD} = 1.5406 Å, Panalytical X’ Pert) radiation, including the high-resolution x-ray reciprocal space mapping (RSM) and transmission electron microscopy (TEM, FEI Tecnai F20). The surface morphology was characterized by atomic force microscopy using the tapping mode (AFM, Vecco, multimode V) and field emission scanning electron microscopy (FESEM, FEI-Apreo-S). Raman (UHT S300 & WITEC), secondary ion mass spectrometry (SIMS, EAG Laboratories in the USA) and SEM-energy dispersive X-ray spectroscopy (SEM-EDS, JED 2300) were also used to analyze the chemical composition. For the Raman analysis, the integration time is 20 s and the spot diameter is 1μm with a 100× objective lens. For the photo-electrical characterizations of the GeSn metal–semiconductor–metal (MSM) photodetectors, the samples were fabricated with conventional lithographic or electron-beam lithographic processes. 100 nm Ti electrode was deposited on GeSn/Ge/Si to form Schottky contact by electron-beam deposition. Photoelectric characteristics were performed using SMU (Keithley 2450) with a 2 μm fiber laser (Thorlabs-FPL2000) on the Probe Station.

3. Results and Discussion

In Figure 1, AFM images were acquired on the GeSn samples with various Sn contents (3.3, 8, and 10%) before and after RTA annealing. The crosshatch patterns (CHPs) are observed on as-grown GeSn with two sets of perpendicular features aligned along two [110]-equivalent directions. Its appearance intensifies and becomes more pronounced with increasing Sn content (Figure 1(a)-(c)).

Furthermore, the spacing of the CHP decreases from 0.8 to 0.25 μm when the Sn content increases from 3.3 to 10%, respectively. Although the 3.3% Sn content sample was annealed at a temperature as high as 700°C, no noticeable change on the surfaces are observed. On the other hand, micro-trenches appear on the 10% Sn content sample annealed at 400°C (Figure S1). It is likely due to the self-running of the Sn-droplet caused by the Sn-segregation [19, 25, 26]. Some immobile Sn-rich droplets appear on the surface of the 8% Sn content samples after annealing at 700°C. However, most areas are free of Sn segregation (see the microscope pictures in Figure S2 and EDS analysis in Figure S3). After the high-temperature annealing process, highly ordered nanopatterns are formed on the hilltop of the crosshatch (Figure 1(e)). The height modulation increases from 8.6 to 16.6 nm (Figures 1(b) and (e)), indicating that surface reconstruction occurs during the high-temperature annealing. Ordered nanopatterns on the annealed 8% Sn-content GeSn were observed by 3D-AFM and SEM as shown in Figure 1(g)-(h) and Figure S4. The surface reconstruction from annealing is frequently observed at the temperature >650°C as well, as shown in Figure S2.

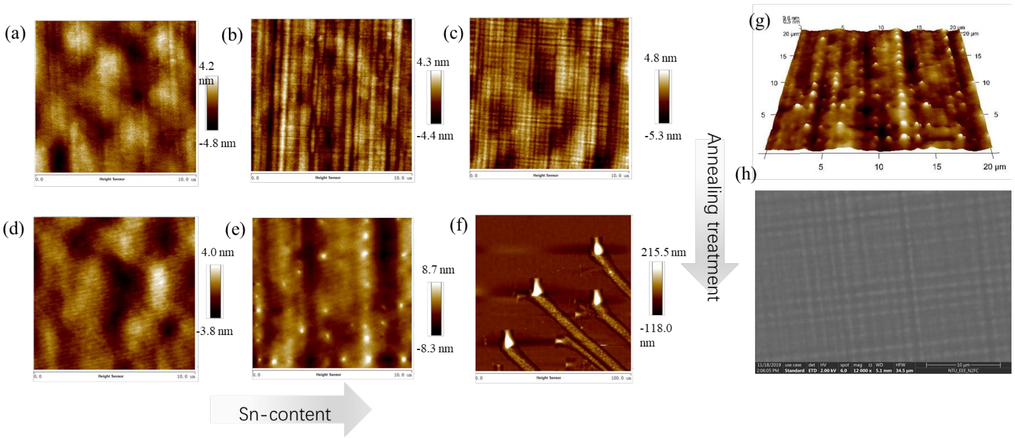

Figure 1. Surface morphology of different Sn-content films before and after annealing treatment. (a) and (d) 3.3% Sn as-grown sample and annealed at 700°C; (b) and (e) 8 % Sn as-grown sample and annealed at 700°C; (c) and (f) 10% Sn as-grown sample and annealed at 400°C; (g) and (h) 3D-AFM and SEM images of the ordered nanopatterns on the annealed 8% Sn-content GeSn sample.

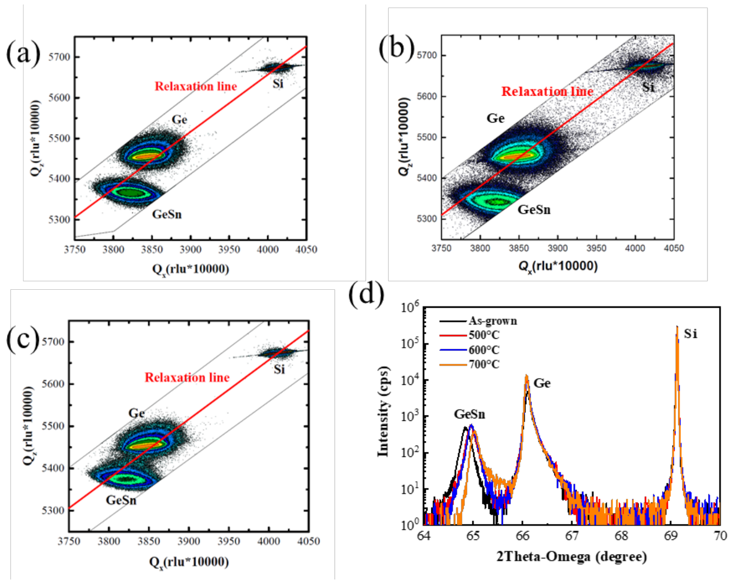

Figure 2. XRD-2DRSM around (224) reciprocal lattice point of GeSn epilayers: (a) and (c) 8 % Sn as-grown and annealing samples(700°C); (b) 10 % Sn as-grown samples; (d) (004) ω-2Θ scans of the 8% Sn samples before and annealing at 500, 600 and 700°C.

To further analyze the Sn incorporation and residual strain of the samples before and after annealing, high-resolution X-ray RSM around the (224) diffractions was performed (Figure 2(a)-(c) and Figure S5). Subsequently, Sn content is estimated according to the procedure developed in Supplementary Material. The macroscopic degree of strain relaxation *R* (%) in all GeSn layers are calculated using the following equation:

$$R(\%) = \frac{a^{//}_{GeSn} - a^{//}_{Ge}}{a_{GeSn} - a^{//}_{Ge}} \qquad (1)$$

where $a^{//}_{GeSn}$ and $a^{//}_{Ge}$ are the in-plane lattice parameters of the GeSn and the Ge layer, respectively, and a_{GeSn} is the relaxed lattice parameter of the GeSn layer. The estimated degree of strain relaxation of the as-grown GeSn with Sn contents of 3.3, 8.0, and 10% is 20, 52, and 47%, respectively. GeSn with higher Sn content has a larger lattice constant and relaxation [27]. The thickness beyond which the larger lattice constant layer cannot accommodate the strain is referred to as the critical thickness (h_c). The People and Bean (P–B) model, which compares the elastic energy stored by the stressed layer and the energy for dislocation nucleation, has been widely used to predict the critical thickness in the SiGe/Si and GeSn/Ge system[28],

$$h_c \approx \left(\frac{1-v}{1+v}\right)\left(\frac{1}{16\pi}\right)\left[\frac{b^2}{a_{GeSn}}\right]\left[\left(\frac{1}{f^2}\right) In\left(\frac{h_c}{b}\right)\right] , \qquad (2)$$

$$f = \frac{a_{GeSn} - a_{Ge}}{a_{Ge}} \ , \qquad (3)$$

where v is the Poisson ratio, b is the length of the Burgers vector. Based on the above equations, the calculated h_c for the 3.3, 8, and 10% Sn-content sample is around 430, 55, and 37 nm. This explains the 3.3% Sn sample has a small strain relaxation with a thickness of 180 nm, while for the high Sn contents samples (8% and 10% Sn) with a similar thickness, more than 50% strain was relaxed. For the 8% Sn sample after 700°C annealing (Figure 2(c)), we found that the decrease in the Sn-content is negligible (~0.14%). However, the compressive strain changes from 0.45 to 0.30% with the strain relaxation increasing from 52 to 69%. Figure 2(d) shows the (004) ω-2Θ scans of the 8% Sn sample after annealing at the temperatures of 500, 600, and 700°C. It shows the right shift of the GeSn peak as the annealing temperature increases, indicating the increase of the strain relaxation.

Based on the above strain analysis, we can explain the occurrences of the CHPs and the ordered nano-patterns on the high Sn-content samples (8 and 10%). The CHP is a common feature for heteroepitaxial systems and has been widely observed in SiGe/Si [29], GaAs/Si [30], and InGaAs/GaAs [31] heteroepitaxial layers. For the growth of GeSn layers, the relaxation process starts with the formation of defects such as misfit dislocations (MDs) on the surface when the thickness beyond the critical thickness. In the heteroepitaxy on (100)-oriented substrates, the strain relaxation is generally completed with the nucleation of MDs at the hetero-interface. In this case, the Burger vectors form a 60° with the <110> direction (Figure 3(a)). These dislocations are glided along the inclined {111} planes. As such, the effect induces a strain inhomogeneity at the free surface along the <110> direction which alters the binding energy of the atoms. According to the linear elastic theory, the binding energy varies linearly with external strain $\varepsilon_{\mathrm{ext}}$ and can be written as [32, 33],

$$E_{ad} = E_{ad0} + A\sigma\varepsilon_{ext} \qquad (4)$$

where E_{ad0} is the binding energy on an unstrained surface, A is the surface area, and σ is the surface stress tensor induced by the adatom. Thus, this modulation strain creates an inhomogeneity atom binding energy on the film surface. As a result, it induces the oriented crosshatch pattern at the film surface (Figure 3(a)).

The dislocation formations at the GeSn/Ge interface were studied by HRTEM. As shown in Figure 3(b) and (c), 60° mixed dislocations are formed near the interface, as shown from the HRTEM image viewed along [110] direction. The corresponding inverse fast Fourier transform (FFT) images are obtained in Fig. 3 (c), confirming the 60° dislocations located at the (111) plane. Due to the low activation energy, 60° dislocations are dominant for the low-temperature (<400°C) epitaxial GeSn layer on Ge [4]. These two MD-induced arrayed lines along the two orthogonal [110]-equivalent directions indicate heavily relaxed strain points when the two vertical lines intersect (Figure 3(a), red dot). At this intersection, the strain relaxation is largest with the highest atom binding energy. Thus, during the high-temperature annealing process for GeSn with the 8% Sn content, the atoms on the film surface tend to migrate to this point to form the ordered nanopatterns, especially when the strain is further relaxed by the thermal effect [18].

The experimental observation of the surface reconstruction (ordered nanopattern) is different from previous works of GeSn films that serious Sn segregation occurs when strain relaxation happens during the annealing process [11,13,15,17]. We also note that some similar reports accounted for the ordered nano-islands or quantum dots (QDs) grown on the surface of heteroepitaxial films. Pandya *et al.* had demonstrated the self-organized, nanoscale 3D-island formation in perovskite thin films due to modulated strain fields [32]. Furthermore, Leon *et al.* and Welsch *et al.* have reported the growth of spatial ordering of InAs QDs strain-relaxed $In_xGa_{1-x}As/GaAs$ layers by utilizing the misfit dislocations [34, 35]. In our work, we only observe the ordered nanopatterns for GeSn with a Sn content of 8%. Typically, high Sn (10%) content GeSn is prone to Sn precipitation when annealed at a temperature higher than 400°C, while for the low-Sn content (3.3%), the low lattice-mismatch from Ge makes the modulated strain fields difficult to form. On other hand, our GeSn sample is relatively thin (<200 nm) compared to GeSn layers of most previous annealing works. Thick GeSn samples are easy to segregate Sn as they have high dislocation density due to the strain relaxation during the growth. Thus, the Sn content and thickness of the film should be optimized to contain the ordered modulation strain and achieve the ordered pattern on GeSn from annealing. This observation of the GeSn surface reconstruction not only shows a new understand of the GeSn material characteristics during annealing but also provides an approach to realize self-patterned 3D nanostructures/QDs for further optoelectronic applications.

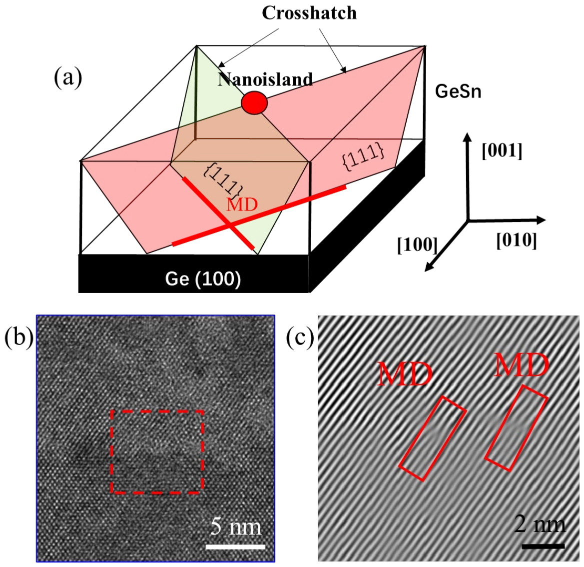

Figure 3 (a) Schematic of the formation mechanism of the crosshatch and ordered nano-island due to the misfit dislocations. (b) The HRTEM image of the $Ge_{0.92}Sn_{0.08}$/Ge interface with Sn-content of 10% along [110] direction. Inside shows the FFT pattern; (c) inverse FFT images were obtained in FFT, showing the extra (111) plane.

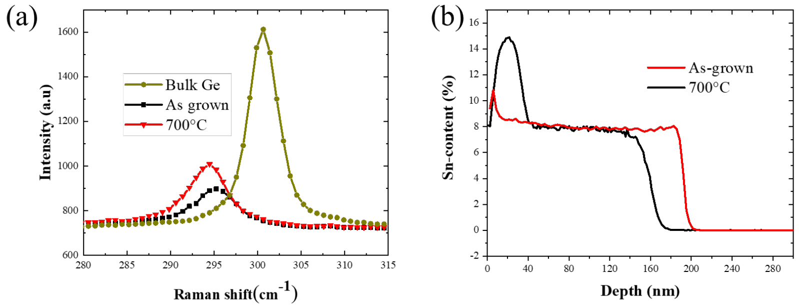

Figure 4. (a) and (b) Raman and SIMS curve of the $Ge_{0.92}Sn_{0.08}$ layer before and after annealing at 700°C.

Micro-Raman spectroscopy with a 532 nm wavelength laser source was performed on the GeSn layers (Figure 4(a)). For the measurement, the input power was set low to avoid the heating effect from the laser source. The spectral of the bulk Ge also was measured under the same power condition. It is important to note that the corresponding penetration depth of a 532 nm laser is around 20 nm in Ge and GeSn. Thus, only the region near the surface of the GeSn layer was measured. The Raman-strain relationship is a function of material composition and strain configuration as follows:

$$\boldsymbol{\Delta\omega = \omega_{Ge} - \omega_{GeSn} = -ax - b\varepsilon} \qquad (5)$$

Here, a is –88 cm^{-1} and b is + 521 cm^{-1} according to Ref. [36] and $\Delta\omega$ is Raman spectral shift variation from 300.4 cm^{-1} (bulk Ge). The as-grown and annealed (700°C) GeSn with 8% Sn content displays the Ge-Ge peaks at 295.3 and 294.5 cm^{-1}, respectively. By substituting the compressive strain of -0.45 and -0.30% estimated from the above XRD-RSM analysis, the Sn-content of the top surface layer of the GeSn sample was obtained to be 8.5% before and after annealing. Thus, the Raman results reasonably match that of the above XRD analysis, indicating the crystallinity of the surface layer. Besides, it is observed the intensity of the Ge-Ge peaks increases obviously after annealing. It might imply that the crystallinity of the GeSn has been enhanced.

SIMS was used to determine the Sn content changes of the GeSn/Ge before and after annealing at 700°C for the 8% Sn-content sample (Figure 4(b)). The measured area was ~100 μm^2 which covers hundreds of crosshatch patterns. As the height of the crosshatch/nanoisland is ~ 10 nm and the analysis depth is ~300 nm, the measurement of the element content will mostly reflect the information of the film. For the as-grown GeSn, the entire GeSn film has a Sn-content around 8%, which is consistent with the above XRD and Raman analysis. However, for the annealed GeSn sample, the Sn content decreases at the GeSn/Ge interface while the Sn content increases at the surface. The total thickness of the GeSn layer decreases from 195 nm to 160 nm after the annealing. The Sn-content decreases at the GeSn/Ge interface might be due to the large lattice-mismatch strain near the interface, which promotes Sn expulsion from the lattice sites. The slop of Sn-content near the interface is less than that of the as-grown GeSn, indicating the tendency to eliminate interfacial strain. On the other hand, the SIMS results show that the Sn-content at the surface is as high as 14% which is higher than those obtained from the Raman spectroscopy and XRD analysis. This is because XRD and Raman only reflect the substitutional Sn concentration in the crystalline Ge. SIMS, on the other hand, includes all the Sn atoms from the GeSn layer.

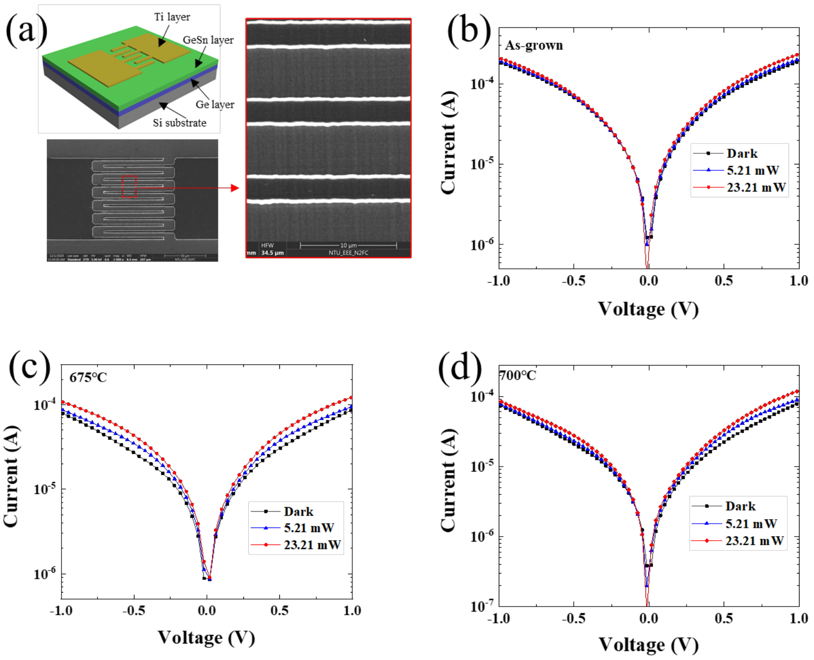

Figure 5 (a) 3d schematic and SEM image of finger-type MSM GeSn device on Ge/Si. (b)-(d) Current-voltage characteristics of the fabricated MSM photodetectors on the as-grown and annealed GeSn at 675 and 700°C measured in dark and under the illumination of 2 μm wavelength with the of 5.21 and 23.21 mW.

To the best of our knowledge, there is no previous work that reports on the effects of thermal annealing on the performance of a single crystal GeSn photodetector . The photocurrent of the GeSn MSM photodetector was measured at 2 μm wavelength with the optical power modulated between 0 to 23.21 mW. A single-mode fiber with a diameter of ~10 μm is coupled from the laser, which is less than the photodetector mesa areas (100*100 μm^2). For the MSM fabrication, the GeSn epilayers (as-grown, annealed GeSn at 675 and 700°C) on Ge/Si substrate were firstly immersed in the buffered oxide etchant (BOE) to remove the Sn or Ge oxide layer. A ~1.5 nm-thick Al_2O_3 layer was then deposited on GeSn epilayers by atomic layer deposition (ALD) at 250°C to alleviate the fermi-level pinning [37]. Interdigitated electrode MSM structures were demonstrated after a ~100 nm Ti deposition on the GeSn epilayers on Ge/Si substrate followed by a lift-off process. The active area is composed of 3 μm interdigitated fingers with 5 μm spacings. The 3D schematic and SEM image of the finger-type MSM GeSn device are shown in Figure 5(a). The nanopattern GeSn surface achieved from annealing could be observed on the active area of the device by SEM. Figure 5(b)-(d) shows the typical current-voltage (I-V) characteristic of the photodetectors before and after the annealing process. It shows that at 2 μm the photocurrent increases when the power intensity increases. The annealing samples (Figure 5(c) and (d)) have a better photon detection performance than the as-grown sample (Figure 5(b)) as indicated by the larger photocurrent to dark current contrast ratio (I_p/I_d ratio) of annealed GeSn photodetectors. At 1V, the dark current of the annealed GeSn photodetectors is suppressed by 62.8 and 66.1% compared to that of the as-grown GeSn photodetector. Furthermore, the photo current at 1 V of the as-grown GeSn, 675 and 700°C annealed GeSn photodetectors are 42.9, 35.8, and 39.8 μA, respectively, with the incident power of 23.21 mW. These photo current values are consistent with our recent study on the flexible GeSn MSM, which has a photon current of 43.6 μA at 2V under the same laser power [38]. These results indicate despite subjecting the samples to high annealing temperatures, the crystal quality of the GeSn has not significantly deteriorated.

Due to the supersaturated vacancy from low-temperature growth, the unintentionally GeSn samples have a p-type background doping. For GeSn, the typical background doping concentrations are around 10^{17} cm^{-3}[38]. For the metal/p-Ge contacts, the hole dark current is consistently high due to the Fermi level pinning at ~0.1 eV near the valence band [37]. Though an ultrathin Al_2O_3 dielectric layer is used to alleviate the Fermi-level pinning, the dark current of the GeSn MSM photodiode is relatively high. Additionally, the device with the large junction area (6.0×10^{-4} cm^2) also aggravates the large dark current. Here, the decrease of the dark current by the high-temperature annealing process might be due to the slightly increased Schottky barrier caused by the elevation of the Fermi level, resulting in the decrease of the hole concentration by the annealing process. Further researches are required to evaluate the changes of the ideality factor, Schottky barrier, and carrier concentration after annealing. A recent study on the amorphous GeSn thin-film also demonstrated a decrease of dark current by a factor of two (from 1 to 0.5 μA) on the MSM photodetector after annealing. It suggests the annealed sample has a lower defect density than that of as-grown samples based on the observation of a decrease of the ideality factor [39].

For the photon current at 2 μm, only the GeSn layer contributes to it as the light absorption by Ge and Si is negligible at 2 μm due to their wider bandgap

(1.1 and 0.8 eV, respectively). The absorption coefficient (α) of Ge at 2 μm is ~1 cm^{-1}, while the strain-free 8% Sn-content GeSn is ~2,100 cm^{-1}[38]. The relationship between absorption and the absorption coefficient ($\boldsymbol{\alpha}$) and thickness of the material (d) is as follows:$\boldsymbol{A(d) = 1 - \exp(-\alpha d)}$.This expression shows the absorption is related to product of the $\boldsymbol{\alpha}$ and *d*. It has been reported that suitable annealing temperature will increase the absorption coefficient of the GeSn film[15]. This is because the annealing accelerates the ion substitution process of Sn atoms in the Ge lattice and decreases the point defect. Additionally, the decrease of the compressive strain from the annealing will also enhance the absorption coefficient due to the shrink of the bandgap of the GeSn and ($\boldsymbol{\alpha \propto \sqrt{hv - E_g}}$). The slightly reduced photon current (from 42.9 to 35.8 and 39.8 μA) might be mainly attributed to the decrease of the thickness of the GeSn. As discussed above, the SIMS results prove that the thickness of the GeSn layer decreases from 195 to 160 nm after the high-temperature annealing at 700°C.

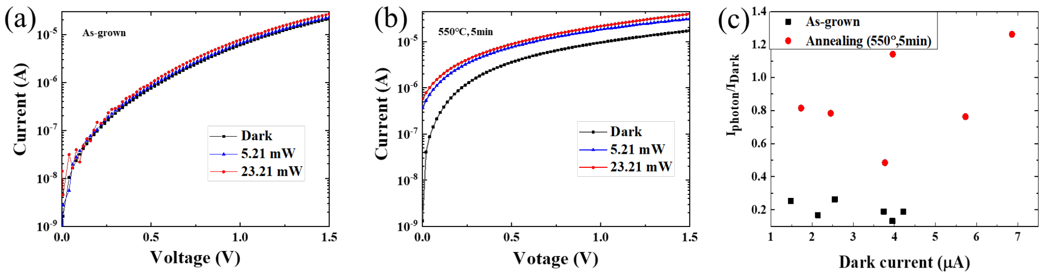

Figure 6. (a) and (b) Current-voltage characteristics of the optimized MSM photodetectors on the as-grown and annealed GeSn at 550°C with 5 minutes measured in dark and under illumination at 2 μm. (c) Ip/Id ratio with the relationship of the dark current at 0.5 V for 12 devices with the input light power of 23.21 mW.

To further enhance the performance of the GeSn photodetector, the size of the device is decreased to obtain a lower dark current, while an optimized annealing temperature is used to enhance the photocurrent. The active area is composed of 1 μm interdigitated fingers with 4 μm spacings with a mesa area of 30x35 μm^2. The total junction area is decreased to 2×10^{-4} cm^2. Annealing at 550°C for 5 minutes was performed on the 8% Sn-content sample before device fabrication. The current-voltage curve of as-grown and annealed GeSn photodetector under dark and light conditions are shown in Figure 6(a) and (b). After annealing, an obvious difference between the dark and light current curve is observed compared to the as-grown sample. For a voltage of 0.5 V, the annealed device has a dark current of 3.6 μA and photocurrent of 4.9 μA (laser power, 23.21 mW), while the as-grown device has the dark and photocurrent of 7.5 and 2.1 μA, respectively. This result indicates that the Ip/Id ratio increased from 0.28 to 1.36 with an obvious photocurrent increase (2.3 times) after an annealing process. It should be noted that the dark, photon current and Ip/Id ratio of initial photodetector annealed at 700°C are 22.3 μA, 7.2 μA, and 0.32, respectively, at 0.5 V (Figure 5 (d)). The obvious dark current decrease (22.3 to 7.5, 3.6 μA) with the decrease of the device size is in line with expectations. On the other hand, the modified device (as-grown and annealed) has a low photocurrent compared to the initial photodetector (2.1 and 4.9 μA compared to 7.2 μA). This is due to a large incident laser spot of a diameter larger than 50 μm, which is larger than the active area of the modified small device. Though the core diameter of the used single-mode fiber is only~10 μm, the incident spot on the device might be larger than 50 μm as the incident light is divergent from a small numerical aperture ~ 0.12 of the fiber [40].

To confirm the increase of photocurrent from annealing, twelve devices (six as grown, six annealed at 550°C) were measured at 0.5 V with the input light power of 23.21 mW. The result shows all annealed devices have a higher I_p/I_d ratio than that of the as-grown sample (Figure 6(c)). The annealed devices have an average I_p/I_d ratio around 0.87 which is 4.4 times of the as-grown device. Furthermore, since the dark currents are on the same scale, the increase of I_p/I_d ratio should be mainly due to the enhanced photocurrent (>2 times) by the annealing process. This result indicates that more electron-hole pairs are created in the thin film, which greatly increases photocurrent. This fact indicates the positive effect of an optimized annealing process on the crystal quality of the GeSn layers and their performance of photodetectors. This optimized temperature is close to the previous GeSn annealing temperature which increases photoluminescent intensities and light absorptions [15, 41]. Finally, it should be pointed out for this annealed condition, the average dark current of the annealed sample (4.08 μA) is slightly higher than that of the as-grown sample (3.01 μA). A reasonable explanation might be the longer annealed time. More research is required to study the effect of annealed time and temperature on the dark current of the GeSn photodetector. For this work, at least, the annealed GeSn photodetector with the same scale of the dark current demonstrates good performance.

4. Conclusion

In summary, we have explored the thermal stability of GeSn epilayers with different Sn contents ranging from 3 to 10% under a series of annealing temperatures (300-750°C). It is observed that highly ordered nanopatterns are formed on the crosshatch GeSn (8% Sn content) surface when the sample is subjected to 700°C RTA for 1 min. These nanopatterns, which consist of ordered 3D-islands are attributed to the redistribution of surface adatoms due to the inhomogeneities of the strain field caused by the periodic misfit dislocations. Despite undergoing high-temperature RTA, these GeSn layers maintain the crystal quality as confirmed by the XRD, Raman, and MSM photodetectors. Furthermore, we also observed a significant photocurrent enhancement (>2 times) when the annealing is carried out at 550°C for 5 min at the wavelength of 2 μm.

This work not only provides an approach to realize self-patterned 3D nanostructures for further optoelectronic applications but also demonstrates a suitable annealing process that will enhance the material quality and photodetector performance of GeSn.

Corresponding Author

E-mail: shaoteng.wu@ntu.edu.sg; TanCS@ntu.edu.sg,

Conflicts of interest

There are no conflicts to declare.

Author Contributions

Chuan Seng Tan and Shaoteng Wu designed the experiments. Lin Zhang and Shaoteng Wu grew the samples. Shaoteng Wu and Bongkwon Son, Qimiao Chen, Hao Zhou, and Simon Chun-Kiat Goh performed the characterizations. Shaoteng Wu wrote the manuscript.

Acknowledgments

This work was support by the National Research Foundation Singapore Competitive Research Programme under Grant NRF–CRP19–2017–01 and Ministry of Education Tier-1 Project under Grant 2019-T1-002-040. We thank the Silicon-Center of Excellence for the use of optical measurement equipment.

Supplementary material

Supplementary data to this article can be found online at

Reference

[1] S. Wirths, R. Geiger, N. von den Driesch, G. Mussler, T. Stoica, S. Mantl, Z. Ikonic, M. Luysberg, S. Chiussi, J.-M. Hartmann, Lasing in direct-bandgap GeSn alloy grown on Si, Nature photonics, 9 (2015) 88-92.

[2] A. Elbaz, D. Buca, N. von den Driesch, K. Pantzas, G. Patriarche, N. Zerounian, E. Herth, X. Checoury, S. Sauvage, I. Sagnes, A. Foti, R. Ossikovski, J.-M. Hartmann, F. Boeuf, Z. Ikonic, P. Boucaud, D. Grützmacher, M. El Kurdi, Ultra-low-threshold continuous-wave and pulsed lasing in tensile-strained GeSn alloys, Nature Photonics, (2020) 375-382.

[3] H. Zhou, S. Xu, Y. Lin, Y.C. Huang, B. Son, Q. Chen, X. Guo, K.H. Lee, S.C. Goh, X. Gong, C.S. Tan, High-efficiency GeSn/Ge multiple-quantum-well photodetectors with photon-trapping microstructures operating at 2 microm, Opt Express, 28 (2020) 10280-10293.

[4] W. Dou, M. Benamara, A. Mosleh, J. Margetis, P. Grant, Y. Zhou, S. Al-Kabi, W. Du, J. Tolle, B. Li, M. Mortazavi, S.Q. Yu, Investigation of GeSn Strain Relaxation and Spontaneous Composition Gradient for Low-Defect and High-Sn Alloy Growth, Sci Rep, 8 (2018) 5640.

[5] R. Loo, Y. Shimura, S. Ike, A. Vohra, T. Stoica, D. Stange, D. Buca, D. Kohen, J. Margetis, J. Tolle, Epitaxial GeSn: impact of process conditions on material quality, Semiconductor Science Technology, 33 (2018) 114010.

[6] S. Assali, J. Nicolas, S. Mukherjee, A. Dijkstra, O. Moutanabbir, Atomically uniform Sn-rich

GeSn semiconductors with 3.0–3.5 μ m room-temperature optical emission, Applied Physics Letters, 112 (2018) 251903.

[7] D. Zhang, L. Jin, J. Li, T. Wen, C. Liu, F. Xu, J. Kolodzey, Y. Liao, MBE growth of ultra-thin GeSn film with high Sn content and its infrared/terahertz properties, Journal of Alloys and Compounds, 665 (2016) 131-136.

[8] V. Richard D’Costa, W. Wang, Q. Zhou, E. Soon Tok, Y.-C. Yeo, Above-bandgap optical properties of biaxially strained GeSn alloys grown by molecular beam epitaxy, Applied Physics Letters, 104 (2014) 022111.

[9] J. Zheng, Z. Liu, Y. Zhang, Y. Zuo, C. Li, C. Xue, B. Cheng, Q. Wang, Growth of high-Sn content (28%) GeSn alloy films by sputtering epitaxy, Journal of Crystal Growth, 492 (2018) 29-34.

[10] O. Nakatsuka, N. Taoka, T. Asano, T. Yamaha, M. Kurosawa, M. Sakashita, S. Zaima, Heteroepitaxial growth of Sn-related group-IV materials on Si platform for microelectronic and optoelectronic applications: Challenges and Opportunities, Ecs Transactions, 58 (2013) 149.

[11] X. Zhang, D. Zhang, B. Cheng, Z. Liu, G. Zhang, C. Xue, Q. Wang, Crystal quality improvement of GeSn alloys by thermal annealing, ECS Solid State Letters, 3 (2014) P127.

[12] H. Li, Y. Cui, K. Wu, W. Tseng, H. Cheng, H. Chen, Strain relaxation and Sn segregation in GeSn epilayers under thermal treatment, Applied Physics Letters, 102 (2013) 251907.

[13] R. Chen, Y.-C. Huang, S. Gupta, A.C. Lin, E. Sanchez, Y. Kim, K.C. Saraswat, T.I. Kamins, J.S. Harris, Material characterization of high Sn-content, compressively-strained GeSn epitaxial films after rapid thermal processing, Journal of crystal growth, 365 (2013) 29-34.

[14] P. Zaumseil, Y. Hou, M.A. Schubert, N. von den Driesch, D. Stange, D. Rainko, M. Virgilio, D. Buca, G. Capellini, The thermal stability of epitaxial GeSn layers, APL Materials, 6 (2018) 076108 .

[15] D. Zhang, Y. Liao, J. Li, T. Wen, L. Jin, X. Wang, J. Kolodzey, Effect of in-situ annealing on the structural and optical properties of GeSn films grown by MBE, Journal of Alloys and Compounds, 684 (2016) 643-648.

[16] C. Comrie, C. Mtshali, P. Sechogela, N. Santos, K. van Stiphout, R. Loo, W. Vandervorst, A. Vantomme, Interplay between relaxation and Sn segregation during thermal annealing of GeSn strained layers, Journal of Applied Physics, 120 (2016) 145303.

[17] C.M. Comrie, C.B. Mtshali, P.T. Sechogela, N.M. Santos, K. van Stiphout, R. Loo, W. Vandervorst, A. Vantomme, Interplay between relaxation and Sn segregation during thermal annealing of GeSn strained layers, Journal of Applied Physics, 120 (2016) 145303.

[18] A. Kumar, J. Demeulemeester, J. Bogdanowicz, J. Bran, D. Melkonyan, C. Fleischmann, F. Gencarelli, Y. Shimura, W. Wang, R. Loo, W. Vandervorst, On the interplay between relaxation, defect formation, and atomic Sn distribution in Ge(1−x)Sn(x) unraveled with atom probe tomography, Journal of Applied Physics, 118 (2015) 025302.

[19] S. Wu, L. Zhang, B. Son, Q. Chen, H. Zhou, C.S.J.T.J.o.P.C.C. Tan, Insights into the Origins of Guided Microtrenches and Microholes/rings from Sn Segregation in Germanium–Tin Epilayers, 124 (2020) 20035-20045.

[20] Z.P. Zhang, Y.X. Song, Y.Y. Li, X.Y. Wu, Z.Y.S. Zhu, Y. Han, L.Y. Zhang, H. Huang, S.M. Wang, Effect of thermal annealing on structural properties of GeSn thin films grown by molecular beam epitaxy, AIP Advances, 7 (2017) 105020.

[21] C.-H. Tsai, B.-J. Huang, R.A. Soref, G. Sun, H. Cheng, G.-E.J.O.I. Chang, GeSn resonant-cavity-enhanced photodetectors for efficient photodetection at the 2 μm wavelength band, 45 (2020) 1463-1466.

[22] S. Xu, W. Wang, Y.-C. Huang, Y. Dong, S. Masudy-Panah, H. Wang, X. Gong, Y.-C.J.O.e. Yeo, High-speed photo detection at two-micron-wavelength: technology enablement by GeSn/Ge multiple-quantum-well photodiode on 300 mm Si substrate, 27 (2019) 5798-5813.

[23] M. Ryu, S. Lee, M. Jang, G. Panin, T.J.J.o.a.p. Kang, Postgrowth annealing effect on structural and optical properties of ZnO films grown on GaAs substrates by the radio frequency magnetron sputtering technique, 92 (2002) 154-158.

[24] S. Rafique, L. Han, H.J.p.s.s. Zhao, Thermal annealing effect on β-Ga2O3 thin film solar blind photodetector heteroepitaxially grown on sapphire substrate, 214 (2017) 1700063.

[25] H. Groiss, M. Glaser, M. Schatzl, M. Brehm, D. Gerthsen, D. Roth, P. Bauer, F. Schäffler, Free-running Sn precipitates: an efficient phase separation mechanism for metastable Ge 1− x Sn x epilayers, Scientific reports, 7 (2017) 1-12.

[26] W. Wang, L. Li, E.S. Tok, Y.-C. Yeo, Self-assembly of tin wires via phase transformation of heteroepitaxial germanium-tin on germanium substrate, Journal of Applied Physics, 117 (2015) 225304.

[27] A. Mosleh, M. Benamara, S.A. Ghetmiri, B.R. Conley, M.A. Alher, W. Du, G. Sun, R. Soref, J. Margetis, J. Tolle, Investigation on the formation and propagation of defects in GeSn thin films, ECS Transactions, 64 (2014) 895.

[28] W. Wang, Q. Zhou, Y. Dong, E.S. Tok, Y.-C.J.A.P.L. Yeo, Critical thickness for strain relaxation of Ge1− x Sn x (x≤ 0.17) grown by molecular beam epitaxy on Ge (001), 106 (2015) 232106.

[29] F. Rovaris, M.H. Zoellner, P. Zaumseil, A. Marzegalli, L. Di Gaspare, M. De Seta, T. Schroeder, P. Storck, G. Schwalb, G. Capellini, F. Montalenti, Dynamics of crosshatch patterns in heteroepitaxy, Physical Review B, 100 (2019) 085307.

[30] T. Nishioka, Y. Itoh, A. Yamamoto, M. Yamaguchi, Crosshatch patterns in GaAs films on Si substrates due to thermal strain in annealing processes, Applied Physics Letters, 51 (1987) 1928-1930.

[31] K.H. Chang, R. Gilbala, D.J. Srolovitz, P.K. Bhattacharya, J.F. Mansfield, Crosshatched surface morphology in strained III-V semiconductor films, Journal of Applied Physics, 67 (1990) 4093-4098.

[32] S. Pandya, A.R. Damodaran, R. Xu, S.L. Hsu, J.C. Agar, L.W. Martin, Strain-induced growth instability and nanoscale surface patterning in perovskite thin films, Sci Rep, 6 (2016) 26075.

[33] L. Huang, F. Liu, X. Gong, Strain effect on adatom binding and diffusion in homo-and heteroepitaxies of Si and Ge on (001) Surfaces, Physical Review B, 70 (2004) 155320.

[34] R. Leon, S. Chaparro, S.R. Johnson, C. Navarro, X. Jin, Y.H. Zhang, J. Siegert, S. Marcinkevičius, X.Z. Liao, J. Zou, Dislocation-induced spatial ordering of InAs quantum dots: Effects on optical properties, Journal of Applied Physics, 91 (2002) 5826-5830.

[35] H. Welsch, T. Kipp, T. Köppen, C. Heyn, W. Hansen, Spatially and energetically resolved optical mapping of self-aligned InAs quantum dots, Semiconductor Science and Technology, 23 (2008) 045016 .

[36] A. Gassenq, L. Milord, J. Aubin, N. Pauc, K. Guilloy, J. Rothman, D. Rouchon, A. Chelnokov, J. Hartmann, V.J.A.P.L. Reboud, Raman spectral shift versus strain and composition in GeSn layers with 6%–15% Sn content, 110 (2017) 112101.

[37] W. Wang, D. Lei, Y.-C. Huang, K.H. Lee, W.-K. Loke, Y. Dong, S. Xu, C.S. Tan, H. Wang, S.-F.J.O.e. Yoon, High-performance GeSn photodetector and fin field-effect transistor (FinFET) on an advanced GeSn-on-insulator platform, 26 (2018) 10305-10314.

[38] S. An, S. Wu, C.S. Tan, G.-E. Chang, X. Gong, M.J.J.o.M.C.C. Kim, Modulation of light absorption in flexible GeSn metal–semiconductor–metal photodetectors by mechanical bending, 8 (2020) 13557-13562.

[39] H. Mahmodi, M.R. Hashim, Effects of post-deposition annealing on crystalline state of GeSn thin films sputtered on Si substrate and its application to MSM photodetector, Materials Research Express, 3 (2016) 106403.

[40] R. Marchetti, C. Lacava, L. Carroll, K. Gradkowski, P. Minzioni, Coupling strategies for silicon photonics integrated chips [Invited], Photonics Research, 7 (2019) 201-239.

[41] N. Taoka, G. Capellini, V. Schlykow, M. Montanari, P. Zaumseil, O. Nakatsuka, S. Zaima, T.J.M.S.i.S.P. Schroeder, Electrical and optical properties improvement of GeSn layers formed at high temperature under well-controlled Sn migration, 70 (2017) 139-144.